Polymer 50 (2009) 4257–4269

Contents lists available at ScienceDirect

Polymer

journal homepage: www.elsevier.com/locate/polymer

A simplified potential energy clock model for glassy polymers☆

Douglas B. Adolf[a,*], Robert S. Chambers[b,1], Matthew A. Neidigk[b,2]

[a] Manufacturing Science and Technology Center, Sandia National Laboratories, PO Box 5800, Albuquerque, NM 87185-1245, USA
[b] Engineering Sciences Center, Sandia National Laboratories, Albuquerque, NM 87185-0893, USA

ARTICLE INFO

Article history:
Received 30 April 2009
Received in revised form
25 June 2009
Accepted 26 June 2009
Available online 3 July 2009

Keywords:
Nonlinear viscoelasticity
Potential energy clock
Yield

ABSTRACT

The potential energy clock (PEC) model for glassy polymers derived previously was shown to predict accurately a broad range of responses including temperature-dependent yield in different modes of deformation, enthalpy relaxation, volume recovery, and aging of the yield stress. It was, however, somewhat difficult to parameterize and employ computationally, and these points may affect its implementation and use. To facilitate acceptance, the model has been greatly simplified by keeping only necessary terms and employing some approximations. The resulting simplified potential energy clock (SPEC) model is quite easily computed and parameterized, yet faithfully reproduces the predictions of the full potential energy clock model implying that experimental responses are still accurately predicted. Such comparisons between the new model, old model, and data are presented as well as new predictions for creep. Again, the predictions are in good agreement with the experimental data.

1. Introduction

Glassy polymers behave viscoelastically. Relaxation rates measured by volume recovery or tensile creep continuously slow as the test temperature decreases below the nominal glass transition temperature, T_g. For polymers cooled quickly below T_g, these relaxation rates slow even at constant temperature as the polymer lethargically strives for equilibrium, leading to numerous phenomena lumped under the heading of "physical aging". Glassy polymers are not simply viscoelastic but are *nonlinear* viscoelastic. Creep rates increase at constant temperature as the applied stress increases, and volumetric relaxation rates depend on the entire volume history.

Theorists have attempted to construct viscoelastic models of glassy polymer response for decades. A number of obstacles have prevented these approaches from being widely applied. First and foremost, many theories attempt to describe only selected pieces of the varied behavior of glassy polymers. For example, free volume [1] and configurational entropy [2] theories, in structure, can predict volume recovery but do not predict the existence of compressive yield. Engineering applications using these models may not require inordinately accurate predictions but need to be "close" (say, to within 20% or so) on *all* predictions to enable design modifications, so exactly predicting room temperature tensile yield while failing to predict any compressive yield would be unacceptable. Even for those models that do attempt comprehensive predictive capability [3], corresponding comprehensive data are lacking. Ideally, one would prefer volumetric, creep, yield, and enthalpic data on a single system with known thermal histories. More detailed descriptions of available viscoelastic theories of glassy polymers with their strengths and weaknesses can be found in our previous publications [4].

In these previous articles [4–7], we developed a nonlinear viscoelastic theory for glassy polymers incorporating two features that enabled comprehensive engineering predictions: use of the logarithmic Hencky strain measure and a novel "material clock" describing the dependence of all relaxation rates on environmental conditions that is based on the potential energy of the system. While seemingly trivial, use of the Hencky strain measure avoided volumetric inconsistencies, which was critically important for glassy polymers whose relaxation rates depend sensitively on volume. The key feature of the new model, however, was use of the "potential energy clock". Since the formalism was based on a Rational Mechanics approach, the potential energy could be constructed consistently. The dependence of relaxation rates on the

☆ Sandia is a multiprogram laboratory operated by Sandia Corporation, a Lockheed Martin Company, for the United States Department of Energy's National Nuclear Security Administration under contract DE-AC04-94AL85000.

* Corresponding author. Tel.: +1 505 844 4773; fax: +1 505 844 9624.
E-mail addresses: dbadolf@sandia.gov (D.B. Adolf), rschamb@sandia.gov (R.S. Chambers), maneidi@sandia.gov (M.A. Neidigk).
[1] Tel.: +1 505 844 0771; fax: +1 505 844 2762.
[2] Tel.: +1 505 844 5845; fax: +1 505 844 2762.

0032-3861/$ – see front matter © 2009 Elsevier Ltd. All rights reserved.
doi:10.1016/j.polymer.2009.06.068

system potential energy was justified in equilibrated systems by molecular dynamics simulations on simple chain molecules [8]. Chain, center-of-mass diffusion coefficients calculated at various temperatures, densities, and pressures and normalized by temperature to construct the mobility collapsed onto a unique master curve when plotted against the system potential energy density, E^{pot}. Moreover, the viscoelastic shift factor, a (proportional to the inverse mobility), apparently diverged at a critical value of the potential energy density, $E^{\mathrm{pot}}{}_{\mathrm{c}}$. The entire functional response could be fit with either a generalized Vogel–Fulcher [9] (or equivalently WLF) equation

$$a = A_1 \exp\left[\frac{A_2}{E^{\mathrm{pot}} - E_{\mathrm{c}}^{\mathrm{pot}}}\right] \tag{1}$$

or with a power law relationship reminiscent of critical phenomena

$$a = A_1 \left[\frac{E^{\mathrm{pot}} - E_{\mathrm{c}}^{\mathrm{pot}}}{E_{\mathrm{c}}^{\mathrm{pot}}}\right]^{-A_2} \tag{2}$$

where A_1 and A_2 are constants in both representations. Finite element predictions using the model for temperature-dependent volume, enthalpy, and yield (compressive and tensile) were in good agreement with data on several systems [5]. Much richer predictions were also shown to agree with data including the dependence of compressive yield on aging time, enthalpy relaxation, and even coupled responses such as the response of the apparent heat capacity for samples that had been previously stressed to yield (enabled by a thermodynamically consistent approach) [7].

While parameterization of the model was related to standard characterization tests, the predictions, at times, were sensitive to the values chosen. Loosely speaking, this sensitivity arose from the very physical foundation of the model; the relaxation rates were dependent on the potential energy of the system, which, in turn, was dependent on the same parameters found in the viscoelastic stress equation. Since the relaxation times were exponentially dependent on the potential energy and, by definition, the viscoelastic relaxation functions were exponentially dependent on the relaxation times, it may not be so surprising that parameter sensitivities arose. These sensitivities were not insurmountable, but we felt that the somewhat complex nature of the equations and the effort required to fit the model accurately might hinder its acceptance. Therefore, we undertook a program to re-examine the model, keeping only those terms necessary for accurate predictions and loosening the tight coupling between clock and stress parameters when possible. In this paper, we describe this process and explain how implementation of the model and subsequent parameterization are now quite simple. Comparison of the simpler model (called here the "Simplified Potential Energy Clock", or SPEC) with both data and the previous, complete model (called the "Potential Energy Clock", or PEC) shows that predictive accuracy was not sacrificed. It is our hope that these efforts will result in a greater willingness to use this model for engineering calculations.

2. Previous theoretical development of the PEC model

Both PEC and SPEC models start from expansion of the Helmholtz free energy, Ψ, in perturbations from an equilibrated state that would exist at the current temperature, T, and density, ρ. The resulting free energy for an isotropic, rheologically simple solid is given by

$$\begin{aligned}\Psi = \Psi_{\mathrm{eq}}(T,\underline{\underline{H}}) &+ \frac{1}{2}\Psi_1 \int_0^t\int_0^t \mathrm{d}s\,\mathrm{d}u f_1\left(t^*-s^*,t^*-u^*\right)\frac{\mathrm{d}I_1}{\mathrm{d}s}\frac{\mathrm{d}I_1}{\mathrm{d}u} \\ &+ \Psi_2 \int_0^t\int_0^t \mathrm{d}s\,\mathrm{d}u f_2\left(t^*-s^*,t^*-u^*\right)\frac{\mathrm{d}\underline{\underline{H}}}{\mathrm{d}s}:\frac{\mathrm{d}\underline{\underline{H}}}{\mathrm{d}u} \\ &+ \Psi_3 \int_0^t\int_0^t \mathrm{d}s\,\mathrm{d}u f_3\left(t^*-s^*,t^*-u^*\right)\frac{\mathrm{d}T}{\mathrm{d}s}\frac{\mathrm{d}I_1}{\mathrm{d}u} \\ &+ \frac{1}{2}\Psi_4 \int_0^t\int_0^t \mathrm{d}s\,\mathrm{d}u f_4\left(t^*-s^*,t^*-u^*\right)\frac{\mathrm{d}T}{\mathrm{d}s}\frac{\mathrm{d}T}{\mathrm{d}u}\end{aligned} \tag{3}$$

where $\underline{\underline{H}}$ is the Hencky strain measure and I_1 is its first invariant, $\underline{\underline{H}}:\underline{\underline{I}}$ (I_2 would be the corresponding second invariant, $\underline{\underline{H}}:\underline{\underline{H}}$). The Hencky first invariant, I_1, is a function of volume only, which, as stated above, avoids volumetric inconsistencies. The expansion prefactors, Ψ_{1-4}, can depend on the current strain and temperature. The underlying equilibrated free energy can also be represented by a Taylor series in strain and temperature about an arbitrary, equilibrated, reference state. The material time, t^*, is dependent on the potential energy of the system, E^{pot}, which was described by a generalized WLF equation

$$t^* - s^* = \int_s^t \frac{\mathrm{d}x}{a(x)} \text{ where } \log a = -C_1\left[\frac{E^{\mathrm{pot}} - E_{\mathrm{ref}}^{\mathrm{pot}}}{C_2' + E^{\mathrm{pot}} - E_{\mathrm{ref}}^{\mathrm{pot}}}\right] \tag{4}$$

where C_1 is identically the familiar WLF constant and C_2' is related to the other one.

All thermodynamic quantities can be found by examining the first and second laws of thermodynamics in terms of the Helmholtz free energy, $\Psi = E - T\eta$, where E is the specific energy and η is the specific entropy.

$$\begin{aligned}&\text{1st Law}: \quad \frac{\mathrm{d}E}{\mathrm{d}t} = \frac{\mathrm{d}W}{\mathrm{d}t} + Q \quad \text{where } \frac{\mathrm{d}W}{\mathrm{d}t} = \frac{\underline{\underline{S}}}{\rho_{\mathrm{ref}}}:\frac{\mathrm{d}\underline{\underline{\Gamma}}}{\mathrm{d}t} \\ &\text{2nd Law}: \quad Q = T\frac{\mathrm{d}\eta}{\mathrm{d}t} - T\frac{\mathrm{d}\eta_{\mathrm{diss}}}{\mathrm{d}t} \\ &\text{such that } \frac{\mathrm{d}\Psi}{\mathrm{d}t} = \left[\frac{\underline{\underline{S}}}{\rho_{\mathrm{ref}}}:\frac{\mathrm{d}\underline{\underline{\Gamma}}}{\mathrm{d}t}\right] - \left[\eta\frac{\mathrm{d}T}{\mathrm{d}t} + T\frac{\mathrm{d}\eta_{\mathrm{diss}}}{\mathrm{d}t}\right]\end{aligned} \tag{5}$$

where $\underline{\underline{S}}$ is the second Piola–Kirchoff stress and $\underline{\underline{\Gamma}}$ is the Green–Lagrange strain measure defined as $1/2(\underline{\underline{F}}^T\underline{\underline{F}} - \underline{\underline{I}})$ with $\underline{\underline{F}}$ being the deformation gradient tensor. The use of $\underline{\underline{\Gamma}}$ for the Green–Lagrange strain measure instead of the more standard nomenclature, $\underline{\underline{E}}$, has been adopted to avoid confusion with the scalar E representing energy. Note that the dissipation rate, $\mathrm{d}\eta_{\mathrm{diss}}/\mathrm{d}t$, must be positive. The rate of change in the Helmholtz free energy then acts as a potential for determining the stress, entropy, and dissipation rate.

$$\begin{aligned}&\frac{\mathrm{d}\Psi}{\mathrm{d}t} = \left(\frac{\partial\Psi}{\partial\underline{\underline{H}}}\right)_T:\frac{\mathrm{d}\underline{\underline{H}}}{\mathrm{d}t} + \left(\frac{\partial\Psi}{\partial T}\right)_{\underline{\underline{H}}}\frac{\mathrm{d}T}{\mathrm{d}t} + \left(\frac{\partial\Psi}{\partial t}\right)_{T,\underline{\underline{H}}} \quad \text{such that} \\ &\underline{\underline{S}} = \rho_{\mathrm{ref}}\left(\frac{\partial\Psi}{\partial\underline{\underline{H}}}\right)_T:\frac{\mathrm{d}\underline{\underline{H}}}{\mathrm{d}\underline{\underline{\Gamma}}} = \rho_{\mathrm{ref}}\,\underline{\underline{\sigma}}_{\mathrm{H}}:\frac{\mathrm{d}\underline{\underline{H}}}{\mathrm{d}\underline{\underline{\Gamma}}}, \quad \eta = -\left(\frac{\partial\Psi}{\partial T}\right)_{\underline{\underline{H}}}, \text{ and} \\ &\frac{\mathrm{d}\eta_{\mathrm{diss}}}{\mathrm{d}t} = -\left(\frac{\partial\Psi}{\partial t}\right)_{T,\underline{\underline{H}}}\end{aligned} \tag{6}$$

where $\underline{\underline{\sigma}}_{\mathrm{H}}$ is the conjugate stress of the Hencky strain. A more rigorous derivation that follows the historical approach of Truesdell

[10] is given in the first paper in this series [1], but the above derivation is intuitively appealing.

The total specific energy can be calculated consistently by $E=\Psi+T\eta$, where Ψ and η are defined in Eqs. (3) and (6). The potential energy is a fraction of the total energy; it can be approximated, however, as detailed in Ref. [1]. Briefly, it was assumed that isothermal volumetric jumps affected changes only in the potential energy, so terms in the expansion of the total energy that involved only volume were included in the potential energy expansion. For isochoric temperature changes, it was assumed that the kinetic energy contribution could be extracted from the total energy by examining the instantaneous response to the temperature jump. This procedure resulted in replacing all prefactors of terms in the expansion of the equilibrated energy involving temperature only with their negative "glassy" values instead of the normal equilibrated values; for example, the equilibrated constant volume heat capacity, $C_{V\infty}$, would be replaced by the negative of its decaying counterpart, $-C_{Vd}$. Limits for the energy expansion cross terms that included both temperature and volume were derived, and comparison of model predictions with data using either of these two limits clearly showed preference for one (again replacing equilibrated terms by the corresponding negative glassy terms).

The resulting constitutive equation (in terms of the Cauchy stress, $\underline{\underline{\sigma}} = (\rho/\rho_{ref})\,\underline{\underline{F}}\cdot\underline{\underline{S}}\cdot\underline{\underline{F}}^T$, required for the momentum balance) is given below.

$$
\begin{aligned}
\underline{\underline{\sigma}} = \rho &\left[\begin{array}{l}
\Psi_1(T,I_1)\displaystyle\int_0^t \mathrm{d}s f_1\left(t^*-s^*\right)\frac{\mathrm{d}I_1}{\mathrm{d}s} \\
+\dfrac{\partial\Psi_1}{2\partial I_1}\displaystyle\int_0^t\int_0^t \mathrm{d}s\,\mathrm{d}u f_1\left(t^*-s^*,t^*-u^*\right)\frac{\mathrm{d}I_1}{\mathrm{d}s}\frac{\mathrm{d}I_1}{\mathrm{d}u} \\
+\Psi_3(T,I_1)\displaystyle\int_0^t \mathrm{d}s f_3\left(t^*-s^*\right)\frac{\mathrm{d}T}{\mathrm{d}s} \\
+\dfrac{\partial\Psi_3}{\partial I_1}\displaystyle\int_0^t\int_0^t \mathrm{d}s\,\mathrm{d}u f_3\left(t^*-s^*,t^*-u^*\right)\frac{\mathrm{d}T}{\mathrm{d}s}\frac{\mathrm{d}I_1}{\mathrm{d}u}
\end{array}\right]\underline{\underline{F}}\cdot\left(\underline{\underline{I}}:\frac{\mathrm{d}\underline{\underline{H}}}{\mathrm{d}\underline{\underline{I}}}\right)\cdot\underline{\underline{F}}^T \\
&+2\rho\underline{\underline{F}}\cdot\left[\begin{array}{l}
\Psi_2(T,I_2)\displaystyle\int_0^t \mathrm{d}s f_2\left(t^*-s^*\right)\frac{\mathrm{d}\underline{\underline{H}}_{\mathrm{dev}}}{\mathrm{d}s} \\
+\dfrac{\partial\Psi_2}{2\partial I_2}\underline{\underline{H}}\displaystyle\int_0^t\int_0^t \mathrm{d}s\,\mathrm{d}u f_2\left(t^*-s^*,t^*-u^*\right)\frac{\mathrm{d}\underline{\underline{H}}}{\mathrm{d}s}:\frac{\mathrm{d}\underline{\underline{H}}}{\mathrm{d}u}
\end{array}\right]:\frac{\mathrm{d}\underline{\underline{H}}}{\mathrm{d}\underline{\underline{I}}}\cdot\underline{\underline{F}}^T \\
&+\rho\left[\begin{array}{l}
\left\{\Psi_{II}+\dfrac{1}{2}\Psi_{III}I_1+\dfrac{1}{2}\Psi_{IIT}\Delta T\right\}I_1 \\
+\left\{\Psi_{IT}+\dfrac{1}{2}\Psi_{IIT}I_1+\dfrac{1}{2}\Psi_{ITT}\Delta T\right\}\Delta T
\end{array}\right]\underline{\underline{F}}\cdot\left(\underline{\underline{I}}:\frac{\mathrm{d}\underline{\underline{H}}}{\mathrm{d}\underline{\underline{I}}}\right)\cdot\underline{\underline{F}}^T \\
&+2\rho\underline{\underline{F}}\cdot\left[\Psi_{HH}+\frac{1}{2}\Psi_{HHT}I_2\right]\underline{\underline{H}}_{\mathrm{dev}}:\frac{\mathrm{d}\underline{\underline{H}}}{\mathrm{d}\underline{\underline{I}}}\cdot\underline{\underline{F}}^T
\end{aligned}
\tag{7a}
$$

where

$$
t^*-s^* = \int_s^t \frac{\mathrm{d}x}{a(x)} \quad\text{and}\quad \log a = -\frac{C_1\left(E^{\mathrm{pot}}-E^{\mathrm{pot}}_{\mathrm{ref}}\right)}{C_2'+E^{\mathrm{pot}}-E^{\mathrm{pot}}_{\mathrm{ref}}}
$$

$$
\begin{aligned}
E^{\mathrm{pot}} = E^{\mathrm{pot}}_{\mathrm{ref}} &+ \left[\begin{array}{l}
\dfrac{1}{2}\Psi_1(T,I_1)\displaystyle\int_0^t\int_0^t \mathrm{d}s\,\mathrm{d}u f_1\left(t^*-s^*,t^*-u^*\right)\frac{\mathrm{d}I_1}{\mathrm{d}s}\frac{\mathrm{d}I_1}{\mathrm{d}u} \\
+\Psi_2(T,I_2)\displaystyle\int_0^t\int_0^t \mathrm{d}s\,\mathrm{d}u f_2\left(t^*-s^*,t^*-u^*\right)\frac{\mathrm{d}\underline{\underline{H}}}{\mathrm{d}s}:\frac{\mathrm{d}\underline{\underline{H}}}{\mathrm{d}u} \\
+\Psi_3(T,I_1)\displaystyle\int_0^t\int_0^t \mathrm{d}s\,\mathrm{d}u f_3\left(t^*-s^*,t^*-u^*\right)\frac{\mathrm{d}T}{\mathrm{d}s}\frac{\mathrm{d}I_1}{\mathrm{d}u} \\
+\dfrac{1}{2}\Psi_4(T)\displaystyle\int_0^t\int_0^t \mathrm{d}s\,\mathrm{d}u f_4\left(t^*-s^*,t^*-u^*\right)\frac{\mathrm{d}T}{\mathrm{d}s}\frac{\mathrm{d}T}{\mathrm{d}u}
\end{array}\right] \\
&+\left[\begin{array}{l}
\dfrac{1}{2}\Psi_{II}I_1^2+\Psi_{HH}I_2-\Psi_3^{\mathrm{ref}}I_1\Delta T-\dfrac{1}{2}\Psi_4^{\mathrm{ref}}\Delta T^2 \\
-\dfrac{1}{2}\left(\dfrac{\partial\Psi_3}{\partial I_1}\right)^{\mathrm{ref}}I_1^2\Delta T-\dfrac{1}{2}\left(\dfrac{\partial\Psi_3}{\partial T}\right)^{\mathrm{ref}}I_1\Delta T^2+\dfrac{1}{6}\Psi_{III}I_1^3 \\
-\dfrac{1}{2}\left(\dfrac{\partial\Psi_4}{\partial T}\right)^{\mathrm{ref}}\Delta T^3-\dfrac{1}{4}\left(\dfrac{\partial^2\Psi_4}{\partial T^2}\right)^{\mathrm{ref}}\Delta T^4+\dfrac{1}{4}\Psi_{HHHH}I_2^2
\end{array}\right] \\
&-T\left[\begin{array}{l}
\Psi_4(T)\displaystyle\int_0^t \mathrm{d}s f_4\left(t^*-s^*\right)\frac{\mathrm{d}T}{\mathrm{d}s} \\
+\Psi_3(T,I_1)\displaystyle\int_0^t \mathrm{d}s f_3\left(t^*-s^*\right)\frac{\mathrm{d}I_1}{\mathrm{d}s} \\
+\dfrac{\partial\Psi_1}{2\partial T}\displaystyle\int_0^t\int_0^t \mathrm{d}s\,\mathrm{d}u f_1\left(t^*-s^*,t^*-u^*\right)\frac{\mathrm{d}I_1}{\mathrm{d}s}\frac{\mathrm{d}I_1}{\mathrm{d}u} \\
+\dfrac{\partial\Psi_2}{\partial T}\displaystyle\int_0^t\int_0^t \mathrm{d}s\,\mathrm{d}u f_2\left(t^*-s^*,t^*-u^*\right)\frac{\mathrm{d}\underline{\underline{H}}}{\mathrm{d}s}:\frac{\mathrm{d}\underline{\underline{H}}}{\mathrm{d}u} \\
+\dfrac{\partial\Psi_3}{\partial T}\displaystyle\int_0^t\int_0^t \mathrm{d}s\,\mathrm{d}u f_3\left(t^*-s^*,t^*-u^*\right)\frac{\mathrm{d}T}{\mathrm{d}s}\frac{\mathrm{d}I_1}{\mathrm{d}u} \\
+\dfrac{\partial\Psi_4}{2\partial T}\displaystyle\int_0^t\int_0^t \mathrm{d}s\,\mathrm{d}u f_4\left(t^*-s^*,t^*-u^*\right)\frac{\mathrm{d}T}{\mathrm{d}s}\frac{\mathrm{d}T}{\mathrm{d}u}
\end{array}\right] \\
&+T\left[\begin{array}{l}
\Psi_4\Delta T+\Psi_3 I_1+\dfrac{1}{2}\left(\dfrac{\partial\Psi_3}{\partial I_1}\right)^{\mathrm{ref}}I_1^2+\left(\dfrac{\partial\Psi_3}{\partial T}\right)^{\mathrm{ref}}I_1\Delta T \\
+\dfrac{3}{2}\left(\dfrac{\partial\Psi_4}{\partial T}\right)^{\mathrm{ref}}\Delta T^2+\left(\dfrac{\partial^2\Psi_4}{\partial T^2}\right)^{\mathrm{ref}}\Delta T^3
\end{array}\right]
\end{aligned}
\tag{7b}
$$

The integral prefactors, $\Psi_{1\text{–}4}$, are respectively related but not identically equal to the difference in the glassy and rubbery bulk moduli ($K_d=K_g-K_\infty$), the difference in the glassy and rubbery shear moduli ($G_d=G_g-G_\infty$), the difference in the glassy and rubbery products of K and the coefficient of thermal expansion, α ($L_d=K_g\alpha_g-K_\infty\alpha_\infty$), and the difference in the glassy and rubbery specific heat capacities at constant volume ($C_{Vd}=C_{Vg}-C_{V\infty}$). Similarly, the elastic model parameters for the equilibrated state, Ψ_{II} and Ψ_{HH}, are related to the rubbery bulk and shear moduli while the quantities, Ψ_{III} and Ψ_{HHHH}, are related to their dependencies on strain. The deviatoric strain is defined as usual by

$$
\underline{\underline{H}}_{\mathrm{dev}} \equiv \left[\underline{\underline{H}} - \frac{1}{3}\left(\underline{\underline{H}}:\underline{\underline{I}}\right)\,\underline{\underline{I}}\right] \tag{8}
$$

The double-valued relaxation functions, $f(t,s)$, can be replaced by the typical single-valued relaxation functions as described in

Appendix B of Ref. [1]. While the derivation of Eq. (7) proceeded simply and accurately predicted a variety of responses for glassy polymers, the resulting expression is quite lengthy, which we feel impedes its acceptance and application. We show in the next section how it can be greatly simplified without loss of predictive accuracy.

3. Simplification of the PEC model

Derivation of the Cauchy stress from the Hencky strain unfortunately requires in Eq. (6) calculation of both a logarithmic strain measure and a fourth-order transformation tensor. While clearly defined and theoretically accurate, this is admittedly complicated and a bit clumsy. In the first simplification, the Hencky strain rate has been approximated by the unrotated rate of deformation tensor, $\underline{\underline{d}}$,

$$\underline{\underline{d}} \equiv \frac{1}{2}\left[\underline{\underline{U}}^{-1}\cdot\frac{\mathrm{d}\,\underline{\underline{U}}}{\mathrm{d}t} + \frac{\mathrm{d}\,\underline{\underline{U}}}{\mathrm{d}t}\cdot\underline{\underline{U}}^{-1}\right] \tag{9}$$

where $\underline{\underline{U}}$ is the stretch tensor obtained from the decomposition of the deformation tensor into its rotation and stretch components, $\underline{\underline{F}} = \underline{\underline{R}}\cdot\underline{\underline{U}}$. Since $\underline{\underline{d}}$ cannot be integrated to obtain a true strain measure, this approach is by definition an approximation. For deformations, however, along principle axes, λ_i, only, such as the standard compressive and tensile tests as well as free expansion, $\underline{\underline{d}}$ and $\mathrm{d}\underline{\underline{H}}/\mathrm{d}t$ produce identical results. In the "1" direction, for example,

$$d_{11} = \frac{\mathrm{d}H_{11}}{\mathrm{d}t} = \frac{\mathrm{d}\lambda_1}{\lambda_1\,\mathrm{d}t} \tag{10}$$

While they differ in more complex modes of deformation, even here the difference is negligible at what would be considered extremely large strains for glassy systems as seen in Fig. 1 in a simple shearing deformation.

While $\underline{\underline{d}}$ can be substituted for the Hencky strain rate to approximate the conjugate Hencky stress, $\underline{\underline{\sigma}}_{\mathrm{H}}$, a transformation to the Cauchy stress is still required, which previously required a cumbersome fourth-order tensor. Examine more closely the approximation to $\underline{\underline{\sigma}}_{\mathrm{H}}$ employing the rate of deformation tensor $\underline{\underline{d}}$ in Eq. (7a). Name this approximate stress $\underline{\underline{\sigma}}_{\mathrm{d}}$.

$$\begin{aligned}\underline{\underline{\sigma}}_{\mathrm{d}} = &\left[K_{\mathrm{d}}\int_0^t \mathrm{d}s\, f_{\mathrm{v}}\left(t^*-s^*\right)\frac{\mathrm{d}I_1}{\mathrm{d}s} - L_{\mathrm{d}}\int_0^t \mathrm{d}s\, f_{\mathrm{v}}\left(t^*-s^*\right)\frac{\mathrm{d}T}{\mathrm{d}s}\right]\underline{\underline{I}}\\ &+ 2G_{\mathrm{d}}\int_0^t \mathrm{d}s\, f_{\mathrm{s}}\left(t^*-s^*\right)\underline{\underline{d}}_{\mathrm{dev}}(s)\\ &+\left[K_\infty I_1 - L_\infty\left\{T-T_{\mathrm{ref}}\right\}\right]\underline{\underline{I}} + 2G_\infty\,\underline{\underline{\varepsilon}}_{\mathrm{dev}}\end{aligned} \tag{11}$$

where the integrated rate has been called, $\underline{\underline{\varepsilon}}$, its first invariant, $\underline{\underline{\varepsilon}} : \underline{\underline{I}}$, is I_1, and the moduli and coefficients of thermal expansion are assumed to be constants thereby allowing direct use of the physical quantities rather than the model prefactors (e.g., K_{d} rather than Ψ_1). The rate of work is independent of the strain measure used so

$$\frac{\mathrm{d}W}{\mathrm{d}t} = \frac{1}{\rho_{\mathrm{ref}}}\underline{\underline{S}} : \frac{\mathrm{d}\,\underline{\underline{T}}}{\mathrm{d}t} = \frac{1}{\rho}\underline{\underline{\sigma}} : \underline{\underline{D}} = \frac{1}{\rho}\underline{\underline{\sigma}}_H : \frac{\mathrm{d}\,\underline{\underline{H}}}{\mathrm{d}t} \approx \frac{1}{\rho_{\mathrm{ref}}}\underline{\underline{\sigma}}_{\mathrm{d}} : \underline{\underline{d}} \tag{12}$$

Using the definition of the rate of deformation tensor, D,

$$\underline{\underline{D}} = \underline{\underline{R}}\cdot\underline{\underline{d}}\cdot\underline{\underline{R}}^T \tag{13}$$

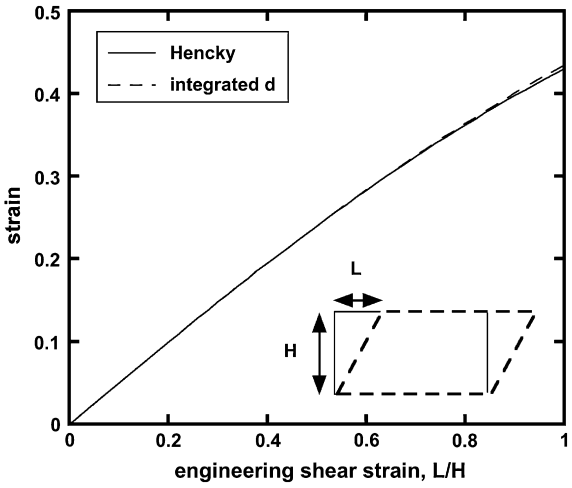

Fig. 1. The Hencky strain is almost identical to the integrated unrotated rate of deformation tensor in a simple shearing deformation to engineering strains of 100%.

the relationship between the true Cauchy stress, $\underline{\underline{\sigma}}$, and the approximate conjugate stress, $\underline{\underline{\sigma}}_{\mathrm{d}}$, can be derived.

$$\frac{1}{\rho}\underline{\underline{\sigma}} : \underline{\underline{D}} = \frac{1}{\rho}\underline{\underline{\sigma}} : \left[\underline{\underline{R}}\cdot\underline{\underline{d}}\cdot\underline{\underline{R}}^T\right] = \frac{1}{\rho}\underline{\underline{\sigma}}_d : \underline{\underline{d}} \quad \text{so}$$

$$\underline{\underline{\sigma}} = \frac{\rho}{\rho_{\mathrm{ref}}}\underline{\underline{R}}\cdot\underline{\underline{\sigma}}_{\mathrm{d}}\cdot\underline{\underline{R}}^T \tag{14}$$

Advantages of constitutive equations directly employing $\underline{\underline{d}}$ were advocated by Flanagan and Taylor [11].

Since deformations along principle axes only involve no rotations, definition of the Cauchy stress using Eq. (14) will produce predictions identical to the PEC model using the Hencky strain. By avoiding use of the logarithmic strain, calculations of stress avoid derivation of the modal matrix and the fourth-order transformation tensor and require only a relatively standard decomposition of the deformation tensor into its rotation and stretch components. In fact, most commercial finite element codes perform this task automatically for the user.

In the next simplification, the dependencies of the moduli and coefficient of thermal expansion (both glassy and rubbery) in the stress equation were minimized to only those proven to this point important for predictive accuracy. The bulk moduli do depend on temperature and density; however, the density dependences are unimportant for most calculations (only becoming relevant in shock applications) and will be eliminated in SPEC. The shear moduli also depend on temperature and could depend on strain through the second invariant. The strain dependence of the glassy shear modulus is required to produce hardening past yield, which is typically not severe. It has been eliminated in the following discussion noting that it could be re-introduced if necessary. The strain dependence of the rubbery shear modulus has not proven important at modest strains (<20%). The coefficients of thermal expansion were allowed to depend on both temperature and density in the PEC model; the volume dependences were suppressed in SPEC since the two effects are similar except again in shock applications.

Another simplification minimized the number of required relaxation functions. In general, four unique relaxation functions are allowed characterizing volumetric (bulk, enthalpy, and CTE) and shear responses. In previous parameterization of unfilled and filled thermosets as well as unfilled thermoplastics using the PEC model, all volumetric relaxation spectra were quite similar while the shear relaxation spectrum was noticeably different. SPEC will

therefore employ only two independent spectra, one volumetric and one shear. The stress equation using these first three simplifications now becomes

$$\underline{\underline{\sigma}} = \frac{\rho}{\rho_{\mathrm{ref}}}\left[K_{\mathrm{d}}(T)\int_0^t \mathrm{d}s f_{\mathrm{v}}\left(t^*-s^*\right)\frac{\mathrm{d}I_1}{\mathrm{d}s} - L_{\mathrm{d}}(T)\int_0^t \mathrm{d}s f_{\mathrm{v}}\left(t^*-s^*\right)\frac{\mathrm{d}T}{\mathrm{d}s}\right]\underline{\underline{I}} + \frac{2\rho G_{\mathrm{d}}(T)}{\rho_{\mathrm{ref}}}\int_0^t \mathrm{d}s f_{\mathrm{s}}\left(t^*-s^*\right)\left[\underline{\underline{R}}(t)\cdot\underline{\underline{d}}_{\mathrm{dev}}(s)\cdot\underline{\underline{R}}(t)^{-1}\right] + \frac{\rho}{\rho_{\mathrm{ref}}}\left[K_\infty(T)I_1 - L_\infty(T)\left\{T-T_{\mathrm{ref}}\right\}\right]\underline{\underline{I}} + \frac{2\rho G_\infty(T)}{\rho_{\mathrm{ref}}}\times\left[\underline{\underline{R}}\cdot\underline{\underline{\varepsilon}}_{\mathrm{dev}}\cdot\underline{\underline{R}}^T\right] \tag{15}$$

The most important simplifications, however, resided in re-definition of the potential energy, which, as seen in Eq. (7b) is quite complex. In general, the potential energy is composed of both first and second-order expansion terms. It was tempting to keep only the first-order terms, which would result in gross simplification. However, it was necessary to keep the second-order deviatoric shear term since it accelerates relaxation rates in response to applied stresses and strains; predictions of nonlinear creep and yield require this term, and without it, the theory mimics a free volume or configurational entropy model, which is rigorously incapable of predicting yield or nonlinear creep in compression. For consistency with the previous simplifications, only the temperature dependence of the model parameters and two relaxation functions were used. The potential energy is now approximated by

$$E^{\mathrm{pot}} \approx E^{\mathrm{pot}}_{\mathrm{ref}} - \frac{TC_{\mathrm{Vd}}(T)}{T_{\mathrm{ref}}}\left[\left\{T-T_{\mathrm{ref}}\right\} - \int_0^t \mathrm{d}s f_{\mathrm{v}}\left(t^*-s^*\right)\frac{\mathrm{d}T}{\mathrm{d}s}\right] - \frac{TL_{\mathrm{d}}(T)}{\rho_{\mathrm{ref}}}\left[I_1 - \int_0^t \mathrm{d}s f_{\mathrm{v}}\left(t^*-s^*\right)\frac{\mathrm{d}I_1}{\mathrm{d}s}\right] + \frac{G_{\mathrm{d}}(T)}{\rho_{\mathrm{ref}}}\int_0^t\int_o^t \mathrm{d}s\,\mathrm{d}u f_{\mathrm{s}}\left(t^*-s^*,t^*-u^*\right)\underline{\underline{d}}_{\mathrm{dev}}(s):\underline{\underline{d}}_{\mathrm{dev}}(u) + \frac{G_\infty(T)}{\rho_{\mathrm{ref}}}\underline{\underline{\varepsilon}}_{\mathrm{dev}}:\underline{\underline{\varepsilon}}_{\mathrm{dev}} \tag{16}$$

The simplifications leading to Eq. (16) were quite severe, and it is therefore doubtful that the prefactors of the potential energy obtained directly from experimental data would yield accurate predictions. A more reasonable path would let these prefactors be adjustable constants whose values are *close* to the theoretical quantities. This final simplification was key to enabling crisp parameterization from limited characterization tests. The potential energy now becomes

$$E^{\mathrm{pot}} = E^{\mathrm{pot}}_{\mathrm{ref}} + E_1\left[\left\{T-T_{\mathrm{ref}}\right\} - \int_0^t \mathrm{d}s f_{\mathrm{v}}\left(t^*-s^*\right)\frac{\mathrm{d}T}{\mathrm{d}s}\right] + E_2\left[I_1 - \int_0^t \mathrm{d}s f_{\mathrm{v}}\left(t^*-s^*\right)\frac{\mathrm{d}I_1}{\mathrm{d}s}\right] + E_3\int_0^t\int_0^t \mathrm{d}s\,\mathrm{d}u f_{\mathrm{s}}\left(t^*-s^*,t^*-u^*\right)\underline{\underline{d}}_{\mathrm{dev}}(s):\underline{\underline{d}}_{\mathrm{dev}}(u) \tag{17}$$

The term containing the equilibrium shear modulus has also been neglected since G_∞ is much smaller than the G_{d} as have the prefactor temperature dependences. Since C_{Vd} and L_{d} are intrinsically negative quantities, the constants, E_{i}, are positive. The viscoelastic shift factor can then be rewritten as

$$\log a = -\frac{C_1 N}{C_2'' + N} \text{ where}$$

$$N = \left[\left\{T-T_{\mathrm{ref}}\right\} - \int_0^t \mathrm{d}s f_{\mathrm{v}}\left(t^*-s^*\right)\frac{\mathrm{d}T}{\mathrm{d}s}\right] + C_3\left[I_1 - \int_0^t \mathrm{d}s f_{\mathrm{v}}\left(t^*-s^*\right)\frac{\mathrm{d}I_1}{\mathrm{d}s}\right] + C_4\int_0^t\int_0^t \mathrm{d}s\,\mathrm{d}u f_{\mathrm{s}}\left(t^*-s^*,t^*-u^*\right)\underline{\underline{d}}_{\mathrm{dev}}(s):\underline{\underline{d}}_{\mathrm{dev}}(u) \tag{18}$$

where

$$C_2'' = \frac{C_2'}{E_1} = C_2\left[1 + C_3\alpha_\infty^{\mathrm{ref}}\right] \cong C_2\left[1 + \frac{T_{\mathrm{ref}}L_{\mathrm{d}}^{\mathrm{ref}}\alpha_\infty^{\mathrm{ref}}}{\rho_{\mathrm{ref}}C_{\mathrm{Vd}}^{\mathrm{ref}}}\right],$$
$$C_3 = \frac{E_2}{E_1} \approx \frac{T_{\mathrm{ref}}L_{\mathrm{d}}^{\mathrm{ref}}}{\rho_{\mathrm{ref}}C_{\mathrm{Vd}}^{\mathrm{ref}}}, \text{ and } C_4 = \frac{E_3}{E_1} \approx -\frac{G_{\mathrm{d}}^{\mathrm{ref}}}{\rho_{\mathrm{ref}}C_{\mathrm{Vd}}^{\mathrm{ref}}} \tag{19}$$

since I_1 is approximately $\alpha_\infty\Delta T$ in free expansion. C_1 and C_2 are the well-known WLF coefficients, while C_3 and C_4 are new clock constants describing the dependence of relaxation times on volume and applied deformations. C_3 will produce a change in the apparent glass transition temperature with pressure and C_4 will produce yield.

Eq. (18) exactly reproduces the historical WLF equation in equilibrated free expansion. When the polymer falls out of equilibrium as it cools below the nominal glass transition temperature in free expansion, Eq. (18) is still applicable since it contains viscoelastic integral terms that naturally reproduce the experimentally observed "leveling-off" of the shift factor. Most interestingly, Eq. (18) accelerates relaxation times by the "C_4" term in the quantity "N", which is the key to engineering calculations by enabling prediction of yield, nonlinear creep, and other important mechanical responses.

For complete clarity, the simplified potential energy clock (SPEC) model equations required to calculate stresses in glassy polymers are collected below.

$$\underline{\underline{\sigma}} = \frac{\rho}{\rho_{\mathrm{ref}}}\left[K_{\mathrm{d}}(T)\int_0^t \mathrm{d}s f_{\mathrm{v}}\left(t^*-s^*\right)\frac{\mathrm{d}I_1}{\mathrm{d}s} - L_{\mathrm{d}}(T)\int_0^t \mathrm{d}s f_{\mathrm{v}}\left(t^*-s^*\right)\frac{\mathrm{d}T}{\mathrm{d}s}\right]\underline{\underline{I}} + \frac{2\rho G_{\mathrm{d}}(T)}{\rho_{\mathrm{ref}}}\int_0^t \mathrm{d}s f_{\mathrm{s}}\left(t^*-s^*\right)\times\left[\underline{\underline{R}}(t)\cdot\underline{\underline{d}}_{\mathrm{dev}}(s)\cdot\underline{\underline{R}}(t)^{-1}\right] + \frac{\rho}{\rho_{\mathrm{ref}}}\left[K_\infty(T)I_1 - L_\infty(T)\left\{T-T_{\mathrm{ref}}\right\}\right]\underline{\underline{I}} + \frac{2\rho G_\infty(T)}{\rho_{\mathrm{ref}}}\left[\underline{\underline{R}}\cdot\underline{\underline{\varepsilon}}_{\mathrm{dev}}\cdot\underline{\underline{R}}^{-1}\right] \tag{20a}$$

where

$$t^*-s^* = \int_s^t \frac{\mathrm{d}x}{a(x)} \text{ and } \log a = -\frac{C_1 N}{C_2'' + N}$$

$$N = \left[\left\{T - T_{\text{ref}}\right\} - \int_0^t \mathrm{d}s\, f_{\text{v}}\left(t^* - s^*\right)\frac{\mathrm{d}T}{\mathrm{d}s}\right] + C_3\left[I_1 - \int_0^t \mathrm{d}s\, f_{\text{v}}\left(t^* - s^*\right)\frac{\mathrm{d}I_1}{\mathrm{d}s}\right] + C_4\int_0^t\int_0^t \mathrm{d}s\,\mathrm{d}u\, f_{\text{s}}\left(t^* - s^*, t^* - u^*\right)\underline{\underline{d}}_{\text{dev}}(s) : \underline{\underline{d}}_{\text{dev}}(u) \tag{20b}$$

Remember that terms, X_{d}, are defined as the difference of the glassy and rubbery values, $X_{\text{g}} - X_\infty$. The relationship between the double-valued shear relaxation function, $f_{\text{s}}(t,s)$, and the typical single-valued, shear stress relaxation function, $f_{\text{s}}(t)$, can be seen clearly by expanding both in a Prony series.

$$\begin{aligned}&\text{if } f_{\text{s}}(t,s) = \sum_k a_k \mathrm{e}^{-t/\tau_k}\,\mathrm{e}^{-s/\tau_k}\\ &\text{then } f_{\text{s}}(t,0) = \sum_k a_k\,\mathrm{e}^{-t/\tau_k} \equiv f_{\text{s}}(t)\end{aligned} \tag{21}$$

While still somewhat complicated, Eq. (20) is now well within reach of anyone serious about predicting the complex responses of glassy polymers. We will show in the next section, that the corresponding parameterization procedure is also well within typical laboratory capabilities.

4. Parameterization of the SPEC model

The ten parameters and two functions required by Eq. (20) are collected in Table 1.

All but two of the constants, C_3 and C_4, are standard inputs to linear viscoelasticity. The bulk moduli can be determined by pressure dilatometry, ultrasonic techniques, or measurements of Poisson's ratio in tension. The shear moduli are easily obtained from commercial rheometers as are the two WLF coefficients and the shear relaxation spectrum. The CTEs are easily obtained from commercial thermomechanical analyzers. Temperature dependencies for all parameters are mild enough to allow representation by a simple linear relationship. The SPEC model parameters can be estimated by extraction from the raw data, but further refinement is suggested by using the model to predict the results of these simple lab tests. This is especially useful for determining the glassy model parameters where the lethargic viscoelastic relaxations can interact with intrinsic temperature dependencies. These computationally modified parameters will typically be slightly different from those obtained by simple extraction from raw data.

Table 1
Parameters required by the constitutive equation.

Symbol	Definition
$K_\infty(T)$	Temperature-dependent equilibrium bulk modulus
$K_{\text{g}}(T)$	Temperature-dependent glassy bulk modulus
$L_\infty(T)$	Temperature-dependent product of K_∞ and the equilibrium CTE, $\alpha_\infty(T)$
$L_{\text{g}}(T)$	Temperature-dependent product of K_{g} and the glassy CTE, $\alpha_{\text{g}}(T)$
$G_\infty(T)$	Temperature-dependent equilibrium shear modulus
$G_{\text{g}}(T)$	Temperature-dependent glassy shear modulus
C_1	First WLF coefficient
C''_2	Related to the second WLF coefficient by $C''_2 = C_2[1 + C_3\alpha_\infty^{\text{ref}}]$
C_3	Determined by the pressure dependence of T_{g}
C_4	Parameter accelerating relaxations by applied deformations
$f_{\text{v}}(t)$	Volumetric relaxation spectrum
$f_{\text{s}}(t)$	Shear relaxation spectrum

The new clock constant, C_3, defines the response of relaxation rates to isothermal volume changes. We have found that C_3 is most easily determined by performing a simple model calculation in which a pressure jump is applied above the nominal (i.e., atmospheric pressure) glass transition temperature, the sample is cooled, and the change in T_{g} in response to the applied pressure is determined. It appears from literature data that the change in T_{g} with pressure for polymers is roughly 0.2–0.4 °C/MPa [5,12]. Therefore, C_3 is simply chosen to reproduce this result. Remember that its value should be *close* to

$$C_3 \approx \frac{T_{\text{ref}}\left[K_{\text{g}}^{\text{ref}}\alpha_{\text{g}}^{\text{ref}} - K_\infty^{\text{ref}}\alpha_\infty^{\text{ref}}\right]}{\rho_{\text{ref}}\left[C_{p_{\text{g}}}^{\text{ref}} - C_{p_\infty}^{ref}\right]} \tag{22}$$

where the measurable constant pressure heat capacity has replaced the constant volume heat capacity of Eq. (19).

This leaves only one parameter, C_4, and the volumetric relaxation function, $f_{\text{v}}(t)$ yet undetermined. As in the PEC model, a stretched exponential form for the volumetric relaxation spectrum will be used in the SPEC model. This assumption is not required.

$$f_{\text{v}}(t) = \exp\left[-\left(\frac{t}{\tau_{\text{v}}}\right)^{\beta_{\text{v}}}\right] \tag{23}$$

Parameterization of this relaxation function therefore requires only two parameters, τ_{v} and β_{v}.

Numerous paths could be suggested for obtaining these remaining three parameters (C_4, τ_{v}, and β_{v}). As in the PEC model, the volumetric spectrum could be obtained by modeling the temperature-dependent CTE as it cools from the equilibrated state through the glass transition and then heated back to the equilibrated state. It is difficult, however, to perform this test on thermoplastics. Likewise, it could be obtained from a similar procedure using the heat capacity, although this would require one to code the SPEC entropy following the same approach as outlined above and parameterize the glassy and rubbery constant volume heat capacities.

$$\eta - \eta_{\text{ref}} = \left[\frac{C_{\text{Vd}}(T)}{T_{\text{ref}}}\int_0^t \mathrm{d}s f_{\text{v}}\left(t^* - s^*\right)\frac{\mathrm{d}T}{\mathrm{d}s} + \frac{L_{\text{d}}(T)}{\rho_{\text{ref}}}\int_0^t \mathrm{d}s f_{\text{v}}\left(t^* - s^*\right)\frac{\mathrm{d}I_1}{\mathrm{d}s} + \text{2nd order terms}\right] + \left[\frac{C_{\text{v}\infty}(T)}{T_{\text{ref}}}\left\{T - T_{\text{ref}}\right\} + \frac{L_\infty(T)}{\rho_{\text{ref}}}I_1 + \text{2nd order terms}\right] \tag{24}$$

While not difficult, it may be unnecessary since the parameter C_4 requires some glassy mechanical test such as yield. It may be easier simply to measure the compressive yield stress at different temperatures and optimize C_4, τ_{v}, and β_{v} to match these data. Creep data might be even better since time dependence is gathered as well, but these tests are typically more difficult and time consuming to perform. If the temperature-dependent compressive yield stresses are used, one wonders about uniqueness and parameter sensitivity. This question will be addressed in the next section. Remember that the value of C_4 should be *close* to the corresponding PEC value

$$C_4 \approx -\frac{\left[G_g^{\mathrm{ref}} - G_\infty^{\mathrm{ref}}\right]}{\rho_{\mathrm{ref}}\left[C_{p_g}^{\mathrm{ref}} - C_{p_\infty}^{\mathrm{ref}}\right]} \tag{25}$$

where again the measurable constant pressure heat capacity has replaced the constant volume heat capacity of Eq. (19).

The parameterization of C_4 highlights an intrinsic difference between the SPEC and PEC models. In the PEC model, the clock faithfully represents the potential energy of the system, and all parameters in the clock originate from linear viscoelastic quantities. Therefore, no nonlinear tests are required to parameterize the PEC model, such that predictions of nonlinear response (e.g., yield and creep) arise from a model with no adjustable parameters. The fact that the PEC predictions agreed with data over a broad range of tests with no adjustable parameters suggested that the underlying physics appeared correct. With the assumptions made in the SPEC model, the parameters in the simplified clock are no longer exactly derived from linear tests, and nonlinear tests (albeit simple yield tests) are required for model parameterization. We feel that this is a small price to be paid for enabling a much simpler constitutive equation and greater flexibility in testing and parameterization. Moreover, the underlying physics (a clock depending on potential energy) have not be abandoned but simply approximated.

5. Comparison of the PEC and SPEC models

In Ref. [5], an unfilled epoxy (DGEBA/DEA with nominal T_g of 70 °C) was fully characterized and used for PEC model validation tests. Predictions of the SPEC model for this epoxy will now be compared to the data and previous PEC model predictions using all parameters from the PEC model except for C_3 and C_4. This comparison will provide a fair assessment of the severity of the assumptions used in deriving the SPEC model. The new SPEC parameters, C_3 and C_4, were determined as suggested in the previous section; C_3 came from a fit of the pressure dependence of T_g, and C_4 came from a fit of the temperature-dependent compressive yield stress. The approximate values of C_3 and C_4 derived from the PEC model and shown in Eqs. (22) and (25) are given in Table 2 as "previous PEC values". While the stretched exponential relaxation exponents (β_1, β_2, β_3) for the bulk modulus, CTE, and heat capacity respectively in the PEC model were identical, the corresponding characteristic relaxation times varied slightly (6 s for the mechanical relaxation times, τ_1 and τ_3, but 20 s for the heat capacity relaxation time, τ_4). The mechanical value of 6 s was used for the SPEC predictions. Parameters used in the PEC and SPEC models are shown in Table 2.

SPEC predictions on four tests detailed in Ref. [5] are shown in Figs. 2–4: the temperature-dependent coefficient of thermal expansion (Fig. 2), the temperature-dependent compressive yield stress (Fig. 3), the difference between tensile and compressive yield at a constant temperature (also shown in Fig. 3), and the temperature-dependent viscoelastic shift factor at different isobaric conditions (Fig. 4). The symbol sizes in these plots give a rough estimate of the errors associated with the tests. The SPEC model predictions reproduce the PEC predictions using all PEC parameters except C_4 (which was slightly reduced), thereby validating the merit of the simplifying assumptions. The only difference seen in the predictions lies in the temperature dependence of the

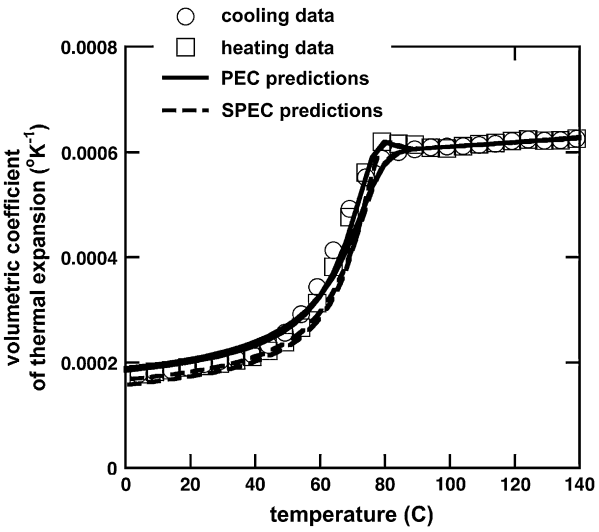

Fig. 2. Comparison of PEC and SPEC predictions and data for thermal expansion.

Table 2
SPEC model parameters for the DGEBA/DEA epoxy.

Parameter	SPEC values used	Previous PEC values	Units
T_{ref}	75	75	°C
$K_\infty(T_{\mathrm{ref}})$	3.2	3.2	GPa
dK_∞/dT	−12	−12	MPa/°C
$K_g(T)$	4.9	4.9	GPa
dK_g/dT	−12	−12	GPa/°C
$\alpha_\infty(T_{\mathrm{ref}})$	600	600	ppm/°C
$d\alpha_\infty/dT$	0.4	0.4	ppm/°C^2
$\alpha_g(T_{\mathrm{ref}})$	170	170	ppm/°C
$d\alpha_g/dT$	0.2	0.2	ppm/°C^2
$G_\infty(T_{\mathrm{ref}})$	4.5	4.5	MPa
dG_∞/dT	0	0	MPa/°C
$G_g(T_{\mathrm{ref}})$	0.75	0.75	GPa
dG_g/dT	−4.2	−4.2	MPa/°C
C_1	16.5	16.5	–
C_2	54.5	54.5	°C
C_3	1000	1000	°C
C_4	8000	11,800	°C
τ_v	6	6	s^{-1}
β_v	0.24	0.24	–
τ_s	0.12	0.12	s^{-1}
β_s	0.22	0.22	–

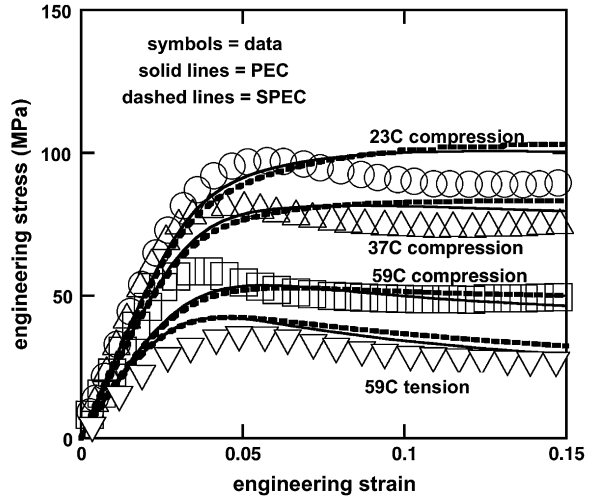

Fig. 3. Comparison of PEC and SPEC predictions and data for the temperature dependence of compressive yield and for the difference between tensile and compressive yield at one temperature.

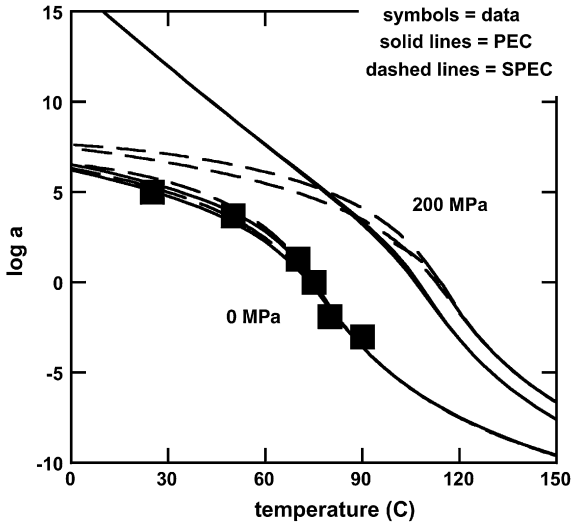

Fig. 4. Comparison of PEC and SPEC predictions and data for the temperature and pressure dependence of T_g.

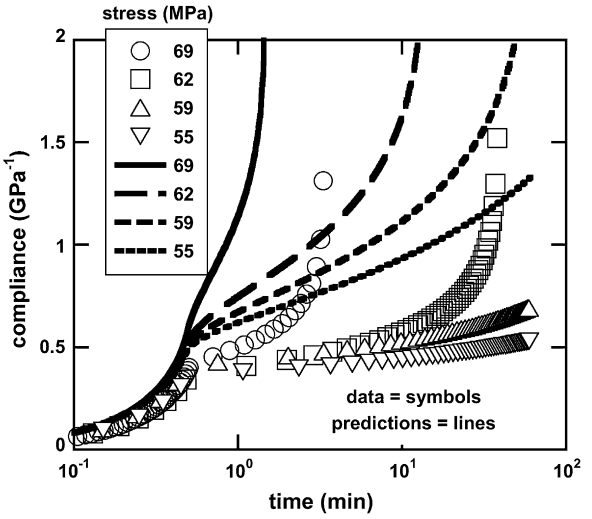

Fig. 6. Creep data and predictions at 23 °C after a slow cool from 100 °C.

viscoelastic shift factor below T_g under pressure. This difference could exhibit itself, for example, in the glassy yield stress under pressure, but no data exist to distinguish between the predictions.

6. New creep predictions of the SPEC model

A series of tensile creep tests at 55 and 23 °C were performed in the present study using the same DGEBA/DEA epoxy (nominal T_g of 70 °C). Two vastly different cooling profiles were used to probe physical aging effects. The dogbone samples (5.1 mm × 12.7 mm cross-section and 57 mm gauge length) were cooled from 100 °C (well above T_g) at rates of 0.5 or 200 °C/min by either cooling in the curing mold as the oven was switched off or by quenching on a cold metal plate. The samples were then transferred to the Instron and tested after a 5 min thermal equilibration time. Both cooling rates were determined by thermocouples located on sample surfaces. While the slower cooling rate measurements were accurate, the faster cooling rates should be viewed as approximate. The faster profiles were not linear, difficult to measure accurately, and might have even produced thermal gradients within the sample. Therefore, the predictions for the slower cooling rates should be viewed quantitatively while the predictions for the quenches should simply be close to the experimental data. Samples were displaced at a constant rate of 5 mm/min using an Instron 1125, screw-driven load frame to determine the tensile yield stresses at room temperature. Displacements were measured with an extensometer directly attached to the dogbone. For creep tests at both test temperatures, the stresses were ramped to the required value in less than one minute, held for 2 h, and if failure did not occur during that period, the stress was released and creep recovery was monitored for another 2 h. Data and predictions for the 23 °C yield response for the different cooling histories are shown in Fig. 5. The creep data are presented in Figs. 6–9. The predictions for the 23 °C tests using the SPEC model with parameters listed in Table 2 are shown in Figs. 6 and 7 as well.

The raw creep data themselves are interesting and deserve some discussion. First, three out of four experimental creep compliances at 55 °C after a slow cool superpose without any time shifting. This suggests that, even though the applied loads approached the measured tensile yield stress at that temperature (roughly 35 MPa), the response is essentially linear viscoelastic.

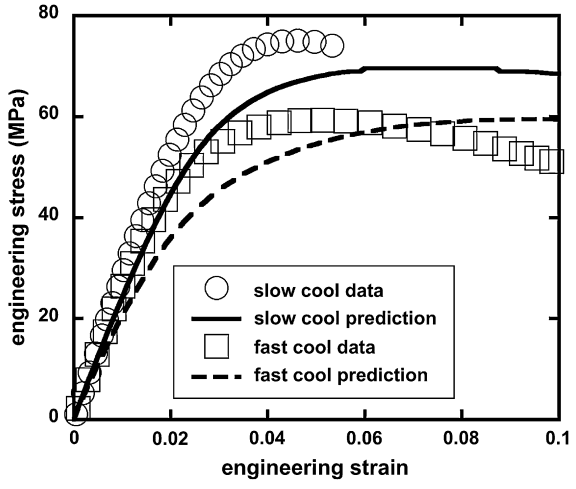

Fig. 5. Comparison of SPEC predictions and data for tensile yield at 23 °C for two different cooling histories.

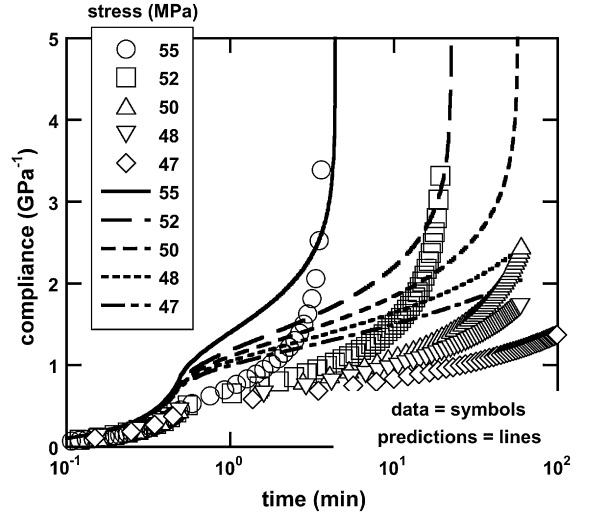

Fig. 7. Creep data and predictions at 23 °C after a fast quench from 100 °C.

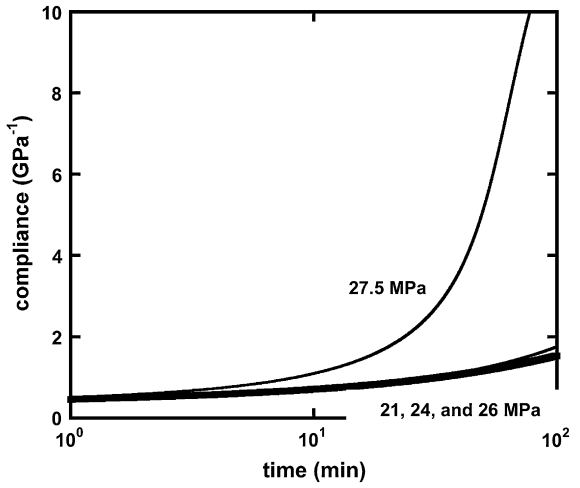

Fig. 8. Creep data at 55 °C (lines) after a slow cool from 100 °C.

That is, the applied stresses are insufficient to produce noticeable acceleration of the relaxation rates at that temperature. At 23 °C, the raw compliances no longer overlap. Older studies in the literature [13] suggested that creep data could be superposed by time shifts dependent upon the applied stress, while more recent studies [14] suggested that master curves could not be constructed. Attempts at master curves for the 23 °C data are shown in Fig. 10. While the two curves at the lowest applied stresses approximately superpose, superposition fails at the higher applied stresses. More interestingly, the shapes of the creep compliances at 23 °C shown in Fig. 10 for the families of samples cooled slowly or quickly are quite distinct.

From a viscoelastic perspective, one would expect superposition of all creep curves (i.e., at all strains and cooling histories) if the polymers were rheologically simple (all relaxation times depending on the same quantities) and if stress accelerated relaxation times (a "stress clock"). In the SPEC model, however, it is not stress exactly that accelerates relaxation rates but the potential energy of the sample. In particular, it is the last term in Eq. (20b) that is responsible for faster decay under applied loads. This last term, in general, involves the double-valued relaxation function, which was represented by a specific form, Eq. (21), in SPEC that reduced it to the more familiar single-valued relaxation function. If instead

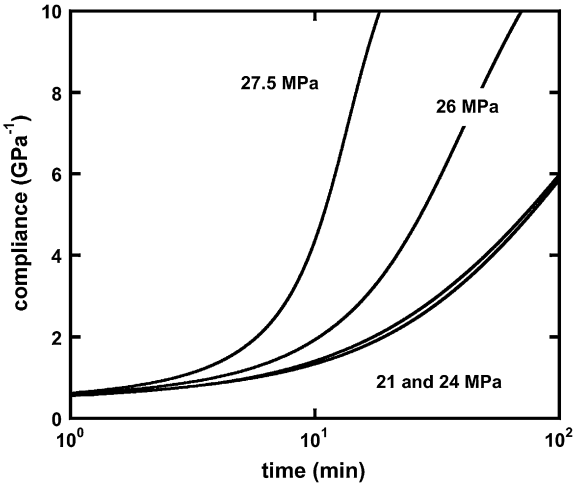

Fig. 9. Creep data at 55 °C (lines) after a fast quench from 100 °C.

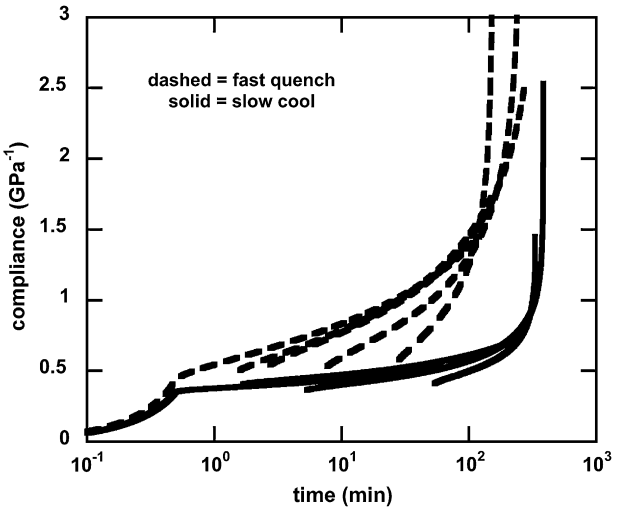

Fig. 10. Attempts at construction of creep master curves from the data at 23 °C (lines) were unsuccessful.

a multiplicative representation for the double-valued relaxation function were used, a stress clock would result

$$\text{if } f(t,s)=f(t)f(s),\quad \int_0^t \mathrm{d}s \int_o^t \mathrm{d}u f_s\left(t^*-s^*,t^*-u^*\right)\underline{\underline{d}}_{\mathrm{dev}}(s):\underline{\underline{d}}_{\mathrm{dev}}(s)$$
$$=\left[\int_0^t \mathrm{d}s f_s\left(t^*-s^*\right)\underline{\underline{d}}_{\mathrm{dev}}(s)\right]:\left[\int_0^t \mathrm{d}s f_s\left(t^*-s^*\right)\underline{\underline{d}}_{\mathrm{dev}}(s)\right]\sim J_2^{\mathrm{dev}} \tag{26}$$

where J_2^{dev} is the second invariant of the deviatoric stress tensor. Interestingly, the multiplicative split is not allowed since it allows negative dissipation rates [15]. This does not imply, however, that a stress clock is strictly disallowed; it simply means that the potential energy term in question cannot be reduced to the second invariant of the stress tensor. A different model altogether might allow a stress clock. On the other hand, remember that the

Table 3
SPEC model parameters used to fit creep data.

Parameter	New creep values	PEC values	Units
T_{ref}	75	75	°C
$K_\infty(T_{\mathrm{ref}})$	3.2	3.2	GPa
$\mathrm{d}K_\infty/\mathrm{d}T$	−12	−12	MPa/°C
$K_g(T)$	4.9	4.9	GPa
$\mathrm{d}K_g/\mathrm{d}T$	−12	−12	GPa/°C
$\alpha_\infty(T_{\mathrm{ref}})$	600	600	ppm/°C
$\mathrm{d}\alpha_\infty/\mathrm{d}T$	0.4	0.4	ppm/°C^2
$\alpha_g(T_{\mathrm{ref}})$	170	170	ppm/°C
$\mathrm{d}\alpha_g/\mathrm{d}T$	0.2	0.2	ppm/°C^2
$G_\infty(T_{\mathrm{ref}})$	4.5	4.5	MPa
$\mathrm{d}G_\infty/\mathrm{d}T$	0	0	MPa/°C
$G_g(T_{\mathrm{ref}})$	0.9	0.75	GPa
$\mathrm{d}G_g/\mathrm{d}T$	−4.2	−4.2	MPa/°C
C_1	16.5	16.5	–
C_2	54.5	54.5	°C
C_3	1000	1000	°C
C_4	11,800	11,800	°C/Pa
τ_v	6	6	s^{-1}
β_v	0.14	0.24	–
τ_s	0.12	0.12	s^{-1}
β_s	0.22	0.22	–

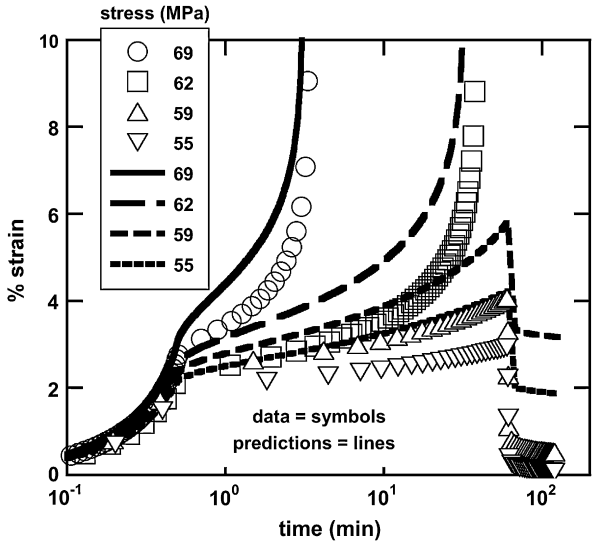

Fig. 11. Creep at 23 °C after a slow cool from 100 °C using new parameters.

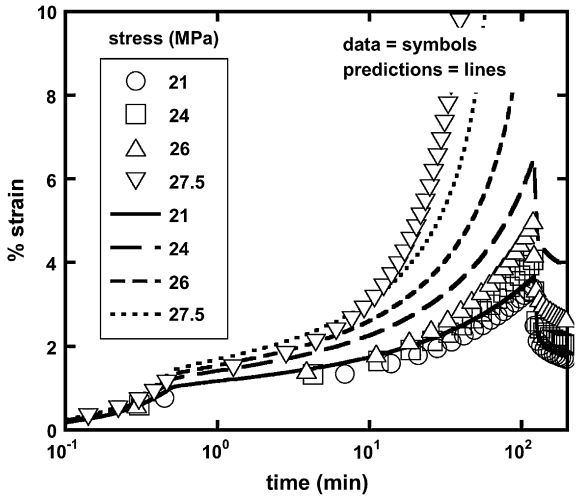

Fig. 13. Creep at 55 °C after a slow cool from 100 °C using new parameters.

molecular dynamics simulations indicated molecular mobility is a unique function of potential energy, so perhaps the stress clock is not rigorously correct.

Now examine the predictions for the 23 °C creep data in Figs. 6 and 7. It is obvious that the SPEC (or equivalently PEC) predictions are not accurate enough. The trends and shapes are correct but quantitative comparison is lacking. Since previous predictions were accurate, one wonders if model re-parameterization could result in better predictions, how different these new parameters might be, and what the effect would be on previous predictions. For example, examination of Figs. 6 and 7 indicate that a slightly larger glassy shear modulus (a simple linear parameter) would improve the fits by lowering the compliance at the end of the stress ramp (roughly 0.7 s). A set of new SPEC parameters derived from fitting the creep data are shown in Table 3 and compared with the PEC parameters from Table 2. The glassy shear modulus was, as suggested, slightly increased, and the only other property requiring adjustment was the exponent describing the volumetric stretched exponential distribution of relaxation times, β_v. Note that the value of C_4 that best fit the creep data was increased back to the PEC value (the SPEC value in Table 2 was 8000). Remember that the three distinct non-shear relaxation spectra of the PEC model were collapsed to a single "volumetric" relaxation spectrum in the SPEC model. For the epoxy system used in this study, the PEC exponents of these three spectra were identical but the relaxation times were different. Perhaps the need for a broader exponent in the SPEC volumetric relaxation spectra (SPEC 0.14 vs. PEC 0.24) is a penalty for reducing the number of relaxation functions. However, since the creep predictions are adequate with a single relaxation function and the assumption eases parameterization considerably, this simplification has been retained. The ordinates in Figs. 11–14 comparing data with predictions have been changed to strain instead of compliance so that recovery after creep can be shown as well.

The creep predictions for all tests are now in much better agreement with the experimental data. The worst agreement is seen at 55 °C for a fast quench (Fig. 14). The fast quench thermal history is approximate as discussed previously, and this uncertainty will manifest itself most severely in this test. While the magnitudes of strain recovery after creep are accurate, the numerical strains

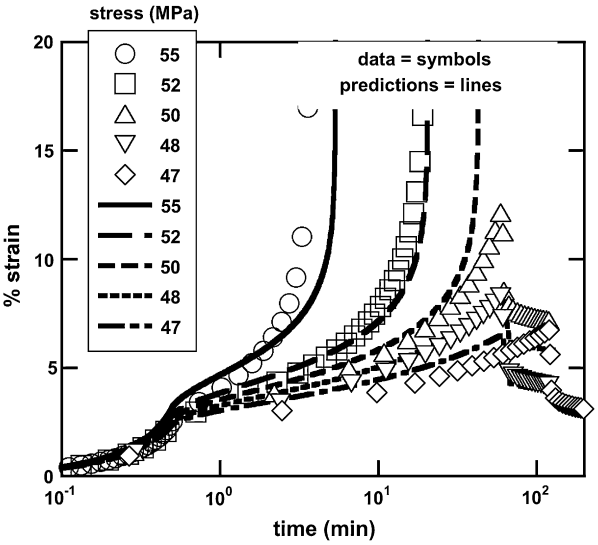

Fig. 12. Creep at 23 °C after a fast quench from 100 °C using new parameters.

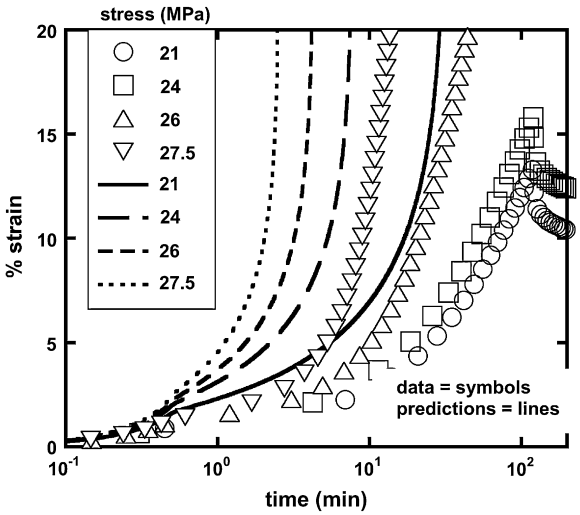

Fig. 14. Creep at 55 °C after a fast quench from 100 °C using new parameters.

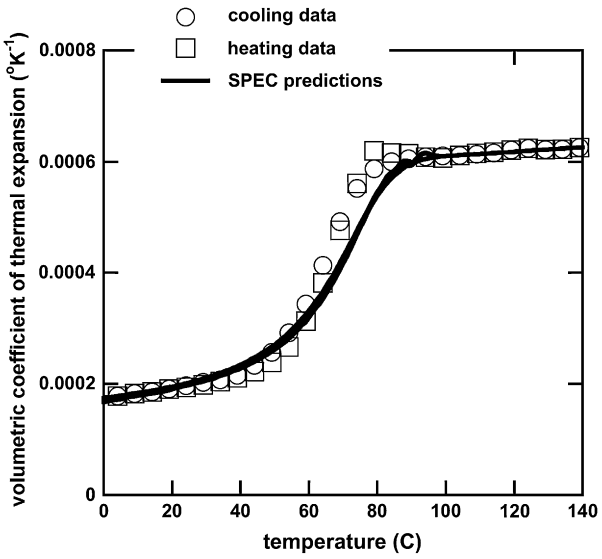

Fig. 15. Comparison of SPEC predictions and data for thermal expansion using new parameters.

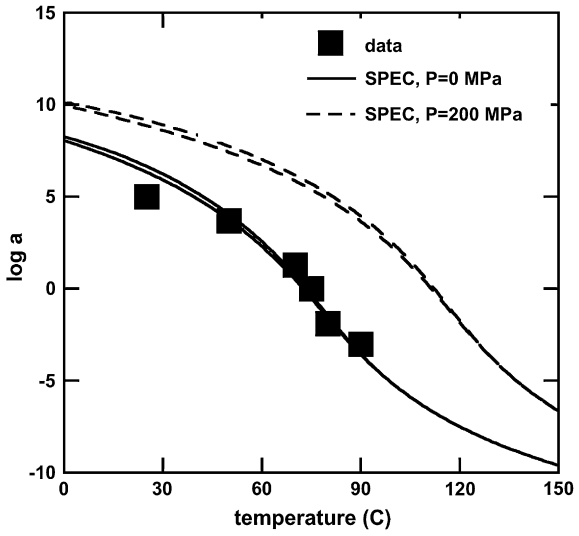

Fig. 17. Comparison of SPEC predictions and data for the temperature and pressure dependence of T_g using new parameters.

predicted during recovery differ in some tests from experiment since the strain at the end of creep is too high (for example, 59 MPa, slow cool, 23 °C). It is apparent that predictions of creep response are much more sensitive to model parameterization than predictions of yield, which is unfortunate since creep tests are more time consuming to perform. Moreover, both the experimental creep response and theoretical predictions are very sensitive to the cooling history, which implies it must be monitored carefully during the tests and modeled accurately in the nonlinear viscoelastic formalism.

The predictions shown previously in Figs. 2–5 are changed only slightly when the new creep parameters are used (Figs. 15–18). In Fig. 15, there is some broadening in the transition of volume with temperature caused by the decrease in value for β_v. The compressive (Fig. 16) and tensile (Fig. 18) yield predictions actually improved significantly.

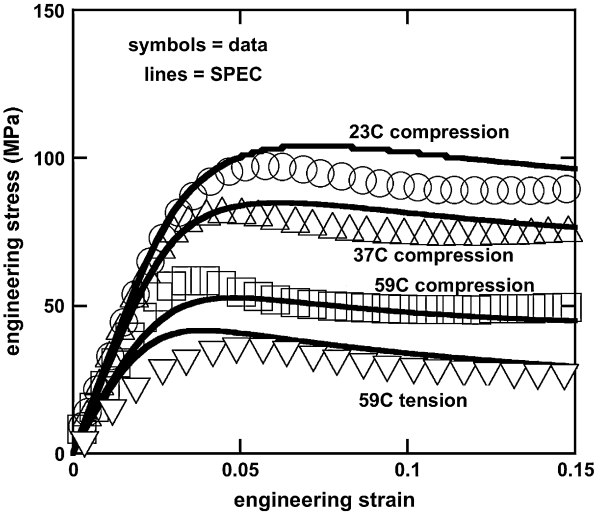

Fig. 16. Comparison of SPEC predictions and data for the temperature dependence of compressive yield and for the difference between tensile and compressive yield at one temperature using new parameters.

7. More complicated predictions of the SPEC model

More complicated PEC model predictions were presented in Ref. [7], and a couple of them will be revisited here using the SPEC model. While the tests are described fully in Ref. [7], they are somewhat involved, so a brief description will be repeated here. In the first test [16], the compressive yield stresses of an epoxy quenched to temperatures 5–20 °C below T_g (roughly 87 °C for this system) were measured as a function of aging time. The yield stresses increased with aging time and then leveled off at aging times that depended on test temperature. In the second test [17], the volumes of two polycarbonate samples (different suppliers with T_g roughly 141 °C) were monitored during a tensile stress relaxation test at room temperature. After the initial increase in volume due to the tensile ramp, the volume decreased during the hold eventually decreasing even below the value of the undeformed sample. Since these test results were extracted from the literature, none of the polymers were characterized. Instead, SPEC model predictions used parameters for the DGEBA/DEA epoxy obtained from fitting creep data (Table 3) with the T_g (or T_{ref}) shifted

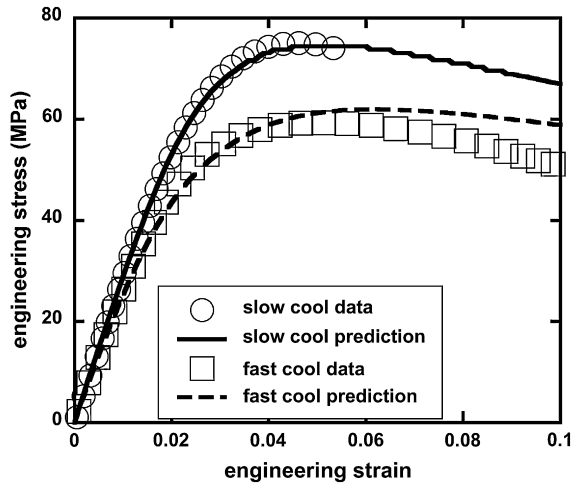

Fig. 18. Comparison of SPEC predictions and data for tensile yield at 23 °C for two different cooling histories using new parameters.

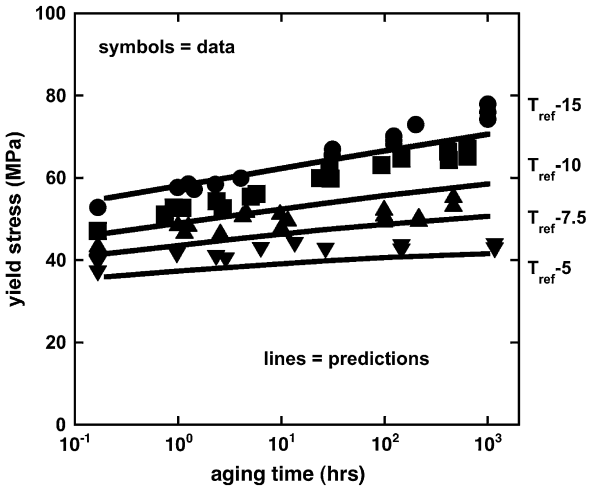

Fig. 19. Data [16] and SPEC predictions for the dependence of the viscoelastic shift factor as a function of aging time.

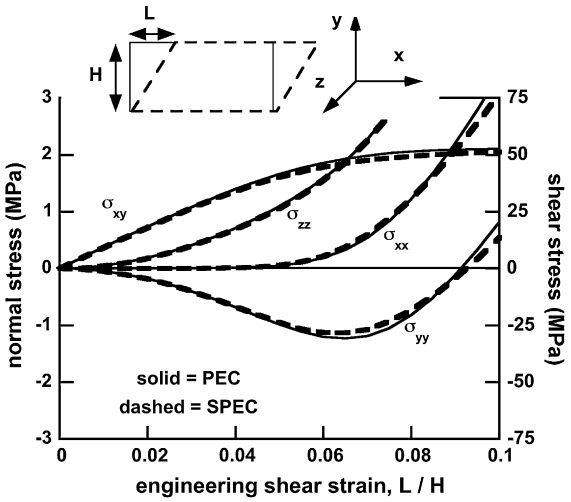

Fig. 21. PEC and SPEC predictions for shear and normal stresses in a simple, one element shear deformation.

to match the experimental systems. Therefore, precise agreement with the data should not be expected. Rather, these more complicated tests show the ability of the model to reproduce complex response: physical aging during both yield and creep tests, and coupled mechanical response (tensile stress and volumetric strain). Since the PEC model predictions qualitatively matched the experimental results in Ref. [7], these tests also offer another opportunity to validate the simplifying assumptions made in deriving the SPEC model. SPEC predictions are compared with experimental data in Figs. 19 and 20.

As explained in Ref. [7], it is not surprising that the volume strain in Fig. 20 decreases below the value prior to application of the tensile strain, V_o. Even prior to the tensile test, the volume is lethargically decreasing toward its equilibrated value. The volume increases with application of the tensile strain (i.e., Poisson's ratio) but will still decrease with time as it tries to reach the equilibrated value. At some point during the test, the volume could certainly decrease below the value at the start of the experiment yet still be far from its equilibrated value.

Another, more complicated challenge for the model lies in prediction of the second-order normal stresses in shear deformations. To assess first any effects from the simplifications made in deriving the SPEC model, a simple shear deformation was imposed on a block of DGEBA/DEA epoxy cooled to 23 °C. Volumetric incompressibility was enforced in the finite element simulation by solving a one element problem in which the separation between the upper (moving) and lower (stationary) faces was fixed and the four nodes on both of these faces maintained their absolute spacings. For fair comparison of the SPEC assumptions, the PEC and SPEC parameters of Table 2 were used since they are almost identical. As seen in Fig. 21, normal stresses are generated, the *yy* normal force in the material at small strains is compressive (i.e., the material is pushing up on the fixed upper plate), all normal forces become tensile after yield, and the predictions from the two models are very similar.

Experimental data on normal forces in glassy polymers are extremely rare, and most of these studies used a rod geometry in which the shear strain varies with the radial position making clear interpretation difficult. One study was uncovered that used tubes of polymethylmethacrylate (PMMA) with an inner diameter of 2.54 cm and outer diameter of 3.81 cm (i.e., a wall thickness of 0.635 cm) [18]. While not exactly "thin" tubes, this geometry does minimize the variation in strain across the sample. The separation between the top and bottom faces was again held fixed, the polymer was adhered to both of these faces, and the bonded

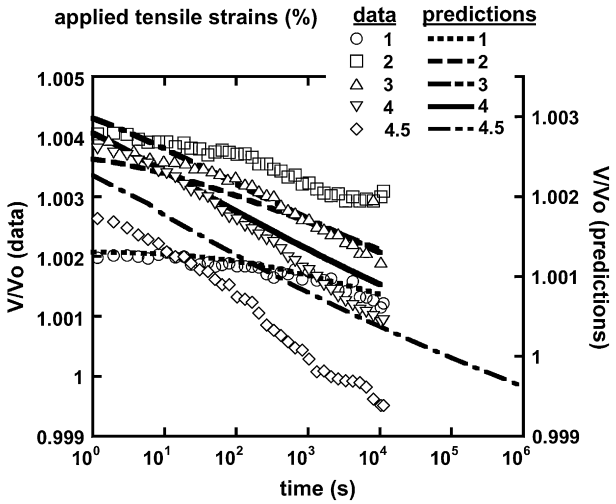

Fig. 20. Data [17] and SPEC predictions for the volume change during a tensile test.

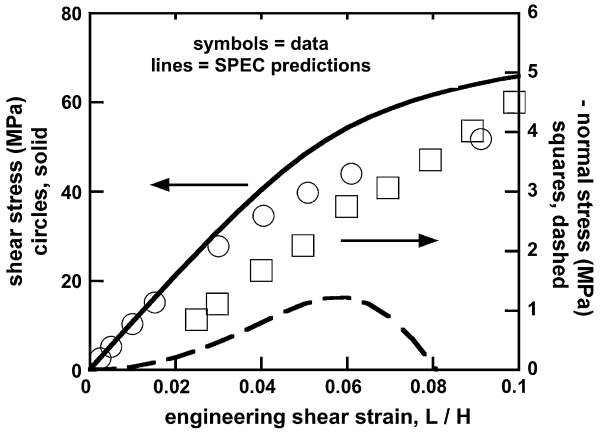

Fig. 22. Data and SPEC predictions for shear and normal forces in torsion of a tube of PMMA at 23 °C.

area was held constant throughout the test. Stresses on the sample faces perpendicular to the *z*-axis were zero, and repeating boundary conditions were applied to the faces perpendicular to the *x*-axis thereby simulating an infinitely long sample (approximating the experimental torsional geometry). The PMMA was approximated using DGEBA/DEA properties from Table 3 (optimized with creep data) with a reference temperature shifted from 75 °C to 100 °C, so comparison with data should be viewed qualitatively. The experimental data and SPEC predictions for a ramp test at 23 °C are shown in Fig. 22, where the shear and normal "stresses" are defined as the total force acting on a surface divided by the surface area. Note also that the normal stress within the material is negative whereas the reported "normal stress" in Ref. [19] is positive. This difference arises from viewing either the stress in the material or the reaction force on the experimental equipment. Normal stresses in polymers are compressive giving rise to the "rod climbing" effects seen in polymeric liquids.

Even with the approximations made in modeling the test geometry and parameterization of the material, the agreement between predictions and experiment is interesting.

8. Conclusions

The potential energy clock model presented and validated in previous papers was greatly simplified. It can now be readily implemented and parameterized by researchers and engineers interested in the nonlinear viscoelastic phenomena of glassy polymers such as yield, nonlinear creep, and physical aging. The simplified potential energy clock still rests on the assumption that all polymer relaxation rates depend uniquely on the system potential energy, which has been verified by molecular dynamics simulations. Predictions of the simplified potential energy clock model were shown to agree well with both the full potential energy clock model and a wide range of experimental data. It is the only model available for glassy polymers that has been shown to reproduce such a wealth of complex responses, and it can be implemented in commercial finite element codes as a user subroutine.

Numerous engineering problems can now be attacked with this model. Examples include prediction of stresses and strains on cool-down from cure (addressing the "stress-free" question), from volumetric relaxations in aging polymers, during creep of load-bearing members, and upon yield around complex geometries in real components (complex tensorial loading). The utility of the model lies in its ability to predict consistently and quantitatively phenomena of importance to practical problems. In addition, the model can be used to enable new perspectives on old research topics in glassy polymers. Examples include cohesive failure (cracking), adhesive failure (de-bonding) failure, filler micro-mechanics, and instabilities. Finally, the approach has already been extended to reacting systems for epoxy cure simulations [19] and is being extended to orthotropic systems for fiber-reinforced polymer composite predictions.

References

[1] See for example: Hutchinson JM, Kovacs AJ. J Polym Sci B 1976;14:1575–90; Chow TS. Macromolecules 1984;17:2336–40; Robertson RE, Simha R, Curro JG. Macromolecules 1984;27:911–9.
[2] See for example: Adam G, Gibbs JH. J Chem Phys 1965;43:139–46; Hodge IM. J Non-Cryst Solids 1994;169:211–66.
[3] See for example: Schapery RA Polym Eng Sci 1969;9:295–310; Knauss WG, Emri I. Polym Eng Sci 1987;27:86–100; Grassia L, D'Amore A. Phys Rev E 2006;74:021504-1.
[4] Caruthers JM, Adolf DB, Chambers RS, Shrikhande P. Polymer 2004;45:4577–97.
[5] Adolf DB, Chambers RS, Caruthers JM. Polymer 2004;45:4599–621.
[6] Adolf DB, Chambers RS. J Polym Sci B 2005;43:3135–50.
[7] Adolf DB, Chambers RS, Flemming J. J Rheol 2007;51:517–40.
[8] Budzien J, McCoy JD, Adolf DB. J Chem Phys 2004;121:10291–8.
[9] Ferry JD. Viscoelastic properties of polymers. New York: Wiley; 1980.
[10] Truesdell C. The elements of continuum mechanics. New York: Springer; 1966.
[11] Flangan DP, Taylor LM. Comput Methods Appl Mech Eng 1987;62:305.
[12] Pantini R. J Appl Polym Sci 2003;89:184–90.
[13] See for example: Struik LCE. Physical aging in amorphous polymers and other materials. Amsterdam: Elsevier; 1978; Crissman JM, McKenna GB. J Polym Sci B 1987;25:1667–77.
[14] Lu H, Knauss WG. Mech Time-Dep Mat 1999;2:307–34.
[15] Golden JM. Int J Eng Sci 2001;39:53.
[16] G'Sell C, McKenna GB. Polymer 1992;33:2103–13.
[17] Colucci DM, O'Connell PA, McKenna GB. Polym Eng Sci 1997;37:1469–74.
[18] McKenna GB, Zapa LJ. J Rheol 1979;23:151–66.
[19] Adolf DB, Chambers RSJ. J Rheol 2007;51:23–50.